Journal Pre-proof

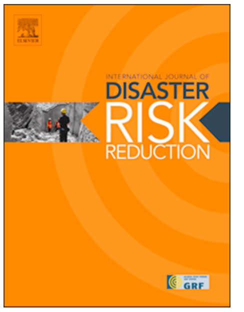

An interactive Web-GIS fluvial flood forecast and alert system in operation in Portugal

Sandra Mourato, Paulo Fernandez, Fábio Marques, Alfredo Rocha, Luísa Pereira

PII: S2212-4209(21)00167-9

DOI: https://doi.org/10.1016/j.ijdrr.2021.102201

Reference: IJDRR 102201

To appear in: *International Journal of Disaster Risk Reduction*

Received Date: 20 January 2021

Revised Date: 16 March 2021

Accepted Date: 16 March 2021

Please cite this article as: S. Mourato, P. Fernandez, F. Marques, A. Rocha, L. Pereira, An interactive Web-GIS fluvial flood forecast and alert system in operation in Portugal, *International Journal of Disaster Risk Reduction*, https://doi.org/10.1016/j.ijdrr.2021.102201.

An interactive Web-GIS fluvial flood forecast and alert system in operation in Portugal

Sandra Mourato[1,4], Paulo Fernandez[2,4], Fábio Marques[3,5], Alfredo Rocha[6] & Luísa Pereira[3,7]

[1] School of Technology and Management, Polytechnic Institute of Leiria. PO Box 4163, 2411-901 Leiria, Portugal

[2] Polytechnic Institute of Castelo Branco, PO Box 119, 6001-909 Castelo Branco, Portugal

[3] Águeda School of Technology and Management, Aveiro University, Rua Comandante Pinho e Freitas, Nº 28, 3750 - 127 Águeda, Portugal

[4] MED – Mediterranean Institute for Agriculture, Environment and Development, Universidade de Évora, Pólo da Mitra, Ap. 94, 7006-554 Évora, Portugal

[5] Institute of Electronics and Informatics Engineering of Aveiro (IEETA), Aveiro University, Portugal

[6] CESAM-Department of Physics, University of Aveiro, Portugal

[7] Research Centre of Geospatial Sciences, Porto University, Porto, Portugal

Abstract: Floods are one of the natural disasters not preventable, affecting people and causing significant damage to economic activities and infrastructures. Thus, it is of foremost importance to, within a disaster risk-reduction strategy, develop a useful flood forecast and alert system to prevent people from suffering flood disasters and mitigate its consequences. This article presents the Flood Forecast and Alert System in operational mode since 2019 for the Águeda river basin located in Portugal's centre region. This system is technologically advanced, differing from others since it uses a coupled real-time hydrologic and 2D hydrodynamic modelling supported on numerical weather prediction and a high-resolution digital terrain surface model. The system components are automatically activated and linked: i) a rainfall forecasting model (WRF), ii) a hydrological model (HEC-HMS), iii) a hydraulic model (HEC-RAS 2D), and a iv) Web-GIS platform. The hydrological model is forced with forecast precipitation for the next three days and updated every six hours, which is crucial to generate pre-flood hazard maps. It also includes a Web GIS service for flood hazard dissemination available for civil authorities and citizens. A flood forecast and alert system is highly relevant to the community since, by enhancing knowledge, it provides the authorities responsible for assessing and managing the flood risk, responsiveness to disasters and timely decision-making, which is even more evident in the context of climate change.

Keywords – flood alert; flood forecasting; flood hazard; hydrological and hydrodynamic modelling; meteorological forecasting; Web services

1 Introduction

Flood events are one of the natural disasters with more impact, affecting people and causing casualties and high economic losses [1-4], whose frequency is likely to increase globally [3, 5-8]. The European Parliament and Council, Directive 2007/60/EC on the assessment and management of flood risk, requires state members to prepare flood hazard and risk maps. Nonetheless, despite the potential that these maps have to help identifying adverse consequences associated with different flood scenarios, the reality is that when a flood event occurs, often citizens barely have time to save their goods or their lives.

Hydrometeorological forecasting is a complex science that links numerical meteorological, hydrological (rainfall-runoff), and hydrodynamic models (flood routing) to forecast the water levels that a flood is expected to reach at particular locations and times [9]. Hydrological models are simplified conceptual representations of the hydrologic cycle and are widely used to produce streamflow forecasts. Hydrodynamic models represent water flow motion using the so-called Navier-Stokes equations, which describe fluid substances' motion in physics [10].

The hydrological models can use as input rainfall data from various sources like rain gauges network, RADAR or simulated precipitation from numerical weather models [11]. Weather forecast is a key component of any forecasting system because it provides timely flood forecast by estimating river flows with sufficient lead-time. High-resolution weather prediction models are now being coupled with hydrological and hydrodynamic models to provide flood hazard forecast assessments at longer lead times incorporated into operational flood forecasting systems [12] such as the European Flood Awareness System [13] and the NOAA's Operational Hydrologic Ensemble Forecast Service [14].

Flood forecast, alert and response are essential components of modern flood preparedness systems. They fall into the category of non-structural flood protection measures, saving lives and reducing material losses and human suffering [15-17] and are essential in a decision support system for operational flood hazard management [18, 19]. Forecast and alert systems can be considered good-practice for Disaster Risk Reduction (DRR), and their importance has been highlighted in global policies like the Sendai Framework for Disaster and Risk Reduction 2015-

2030 [20]. Incorporating forecasting and alert systems into DRR strategies increase community resilience to natural disasters empowering citizens and communities to respond appropriately.

Flood forecast and alert systems are increasingly being developed and used worldwide [21]. Frequently, an Early Warning System (EWS) is built on flood projections based on either real-time automatic water level monitoring [22], real-time hydrologic modelling [11, 13, 23-25], real-time hydrodynamic modelling [26, 27] or real-time hydrologic and hydrodynamic modelling [28, 29] with a lead time depending on the basin hydrological response. Several systems are based on meteorological weather forecast [13, 25, 27, 29, 30] or on using high-resolution altimetric data as Light Detection And Ranging (LiDAR) [27, 28]. The Portuguese EWS with the designation SVARH [22] and available on (https://snirh.apambiente.pt/index.php?idMain=2&idItem=5.1) does not contain weather forecast or flood modelling; instead, the flood forecast is made in real-time as they rely on water levels observations. The Delft-FEWS [31] provides an operational forecasting platform through which different model codes can be brought to the operational domain. These models can then be linked with data imported from various external databases and many different file formats. This platform has a user's community in several countries of the world.

There are several zones regularly flooded in Portugal, often with severe consequences. Águeda, a small town in Portugal's centre region, with a drainage area of 408 km^2, is included in the national list of the critical flooded zones [32]. Its urban area, crossed by the river with the same name, is one of the areas with the highest number of flood occurrences causing property damage and even human losses [33]. Águeda municipality has made, in 2015, a considerable investment of around two million euros in the construction of a secondary river channel to divert the river flow. This channel on the left bank of the Águeda river has an extension of 791 m, 2.68 m depth and a 22 m width. It was designed to prevent floods for a 20 years return period (231.06 m^3/s) together with the main river. Regrettably, it did not totally mitigate the impact of flooding. Three of the most significant flood events from the last 15 years affected the region in February 2016, February 2019 and December 2019. The short lead-time between the rain and the flood makes it very difficult to issue early warnings or take safety measures once the rain starts. The best option is to forecast the possibility of a flood before it occurs, enabling defensive actions to be taken well in advance. Thus, this paper's main objective is to present the Flood Forecast and Alert System (FFAS) developed to forecast well in advance fluvial floods in the Águeda river basin using meteorological forecasting. The main advantage of this system is that it coupled real-time hydrologic and 2D hydrodynamic modelling supported on Numerical Weather Prediction

(NWP), a high-resolution digital terrain surface model, and the flood forecasts are disseminated through a Web-GIS updated every 6 hours

2 Study area and data

The study area is located in Águeda municipality in the centre of Portugal (Figure 1a). It corresponds to 560 ha, crossed by a stretch of 9.8 km of the River Águeda, including Águeda city centre and the artificial channel constructed to deviate the riverbed water. The area was delimited considering the 100 years return period flood extent defined by the National Water Authority and extended to include the steep slopes ensuring the full possible flood extent. The river is mainly surrounded by agricultural fields bordering hillslopes that are typically steep, with angles of 16–25% and >25% in, respectively, 9 and 14% of the area [34]. The river margins have riparian vegetation with an elevated density, consisting of trees such as the alder, elm, oak, chestnut, and shrubs such as elderberries, holly, laurel, black alder, heather, and gorse. The study area elevation varies between 1 to 70 m (Figure 1e).

The river basin contributing to the study area occupies 408 km^2, and the elevations of the catchment range between 10 and 1070m (Figure 1b). Its area, crossed by Águeda River, has the highest number of flood occurrences facilitated by Serra do Caramulo steep slopes, where Águeda River rises, having mainly large impervious alluvial areas in its entire catchment. According to the Köppen e Geiger climatic index, the region is classified as Csb (Warm-summer Mediterranean climate). The mean annual rainfall is 1800 $mm.y^{-1}$, with a strong inter□annual variability ranging from 1,100 to 2,700 $mm.y^{-1}$. There is a strong seasonal contrast with 70% of the rainfall in autumn and winter. Stormflow generation is driven by saturation□excess in the wet season due to higher rainfall amounts and wetter catchment conditions. The land use of the catchment consists of eucalypts and maritime pines forest (76%), small agricultural fields (10%), scrub (9%) and urban areas (4%) (Figure 1c). Soils are generally shallow, and the main soil type is Cambisols (Figure 1d), developed over schist and granite bedrocks and characterised by a high saturated hydraulic conductivity of about 30-40 $mm.h^{-1}$ [35].

Besides the aspects that tamper the runoff flow, there is still the side effect of forest fires ravaging Caramulo, occurring almost every year with different burned area extent. During the last years, significant forest fires occurred; 2013 (7 794 ha), 2016 (5 698 ha) and 2017 (8 458 ha), corresponding respectively to 19%, 14% and 21 % of the river basin. As the vegetation is burned, the precipitation contributes to significant soil erosion, dragging eroded and burned material into the river. This material accumulates and hinders the flow that can reach hydrometric historical levels with minor quantitative precipitation. The flooding probability is expected to increase due to the climate change projections, with the amount of rainfall expected to be concentrated in smaller periods [36, 37].

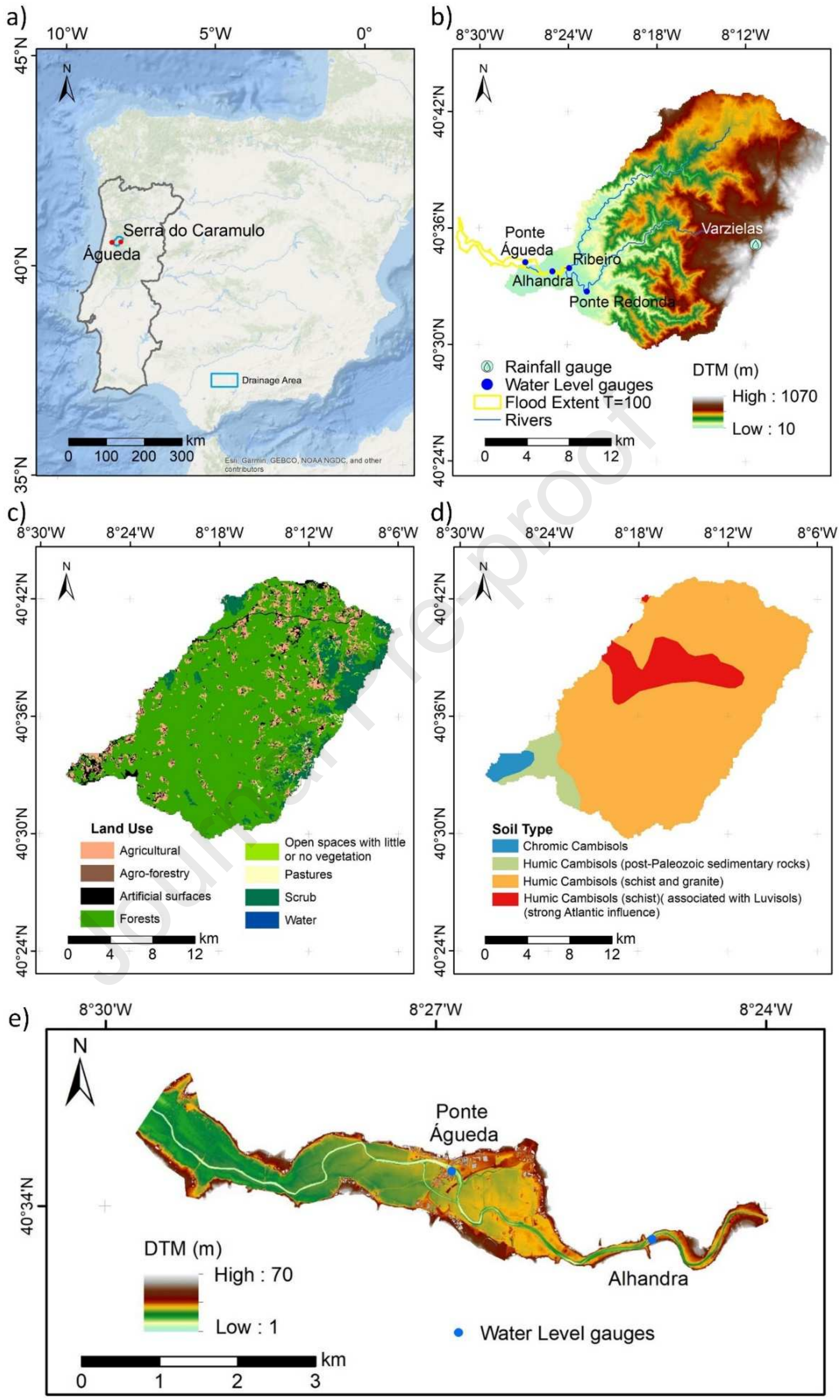

Figure 1. a) Location of Águeda River basin. b) DTM of Águeda river basin, including water level and rainfall gauges and flood extension for the 100 years return period. c) Águeda river basin main land uses; d) Águeda river basin soil types. e) DTM of the flood forecast study area and water level gauges location.

The data presented here are needed to calibrate and validate the meteorological and hydrodynamic models and run the system in an operational mode. The meteorological model (section 3.1) and the hydrological model (3.2) was calibrated and validated with rainfall data from the National Environmental monitoring network collected from the Varzielas rainfall gauge in the Caramulo mountain (Figure 1b)). For calibration and validation, the hydrological model uses streamflow data from three water level gauges (Figure 1b) from the National Environmental monitoring network: i) Ponte de Águeda (in the city downtown), ii) Ponte Redonda (in the Águeda River upstream the city centre), iii) and Ribeiro (in the Alfusqueiro River, a tributary of the Águeda River upstream the city centre). The data set included hourly data from all the gauges for 2007 to 2018. During the FFAS development, a water level gauge was installed in 2018 (Alhandra, Figure 1b and 1e) near the upstream boundary of the hydrodynamic study area, 3 km upstream of the Ponte de Águeda gauge to provide data for the hydrodynamic model calibration and validation. The flow curve was estimated for that location based on the pair values of hydrometric height and flow measured in the river section. The hydrodynamic model was calibrated and validated against the Ponte de Águeda and Alhandra water level records.

For the river basin hydrological modelling, the terrain topography is represented by a Digital Terrain Model (DTM), Figure 1b, obtained from Shuttle Radar Topography Mission (SRTM) version 3.0 with a spatial resolution of 30 meters [38]. The land cover and soil type spatial data to compute the Curve Number (CN) (section 3.2) are the COS2018 and the European Soil Database v2 Raster. COS2018 is a land cover map available at a 1:25,000 scale and has a minimum mapping unit of 1 ha and a classification system with 83 classes [39]. The European Soil Database v2 Raster is a raster data with a cell size of 1 km x 1 km [40].

The topographic and land use data used in the hydrodynamic modelling were obtained with LiDAR and aerial images, both acquired by UAV (Unmanned Aerial Vehicles). The terrain surface is a critical factor in flood modelling because the hydrodynamic model conditions the flood hydrograph and the flood extent [41-44]. Concerning the study area, the terrain topography and thematic information were derived from LiDAR data and aerial images, both acquired by UAV. LiDAR data provide high-resolution altimetric data and characterise the surface topography of flood-prone areas, which are important input data for flood modelling [41, 45-47]. The LiDAR data acquisition was carried out between 22 and 25 January 2018, and it involved 42 flights at a mean flying height of 50 m.

The system used consisted of a platform, the UAV DJI Matrice 600 Pro Hexacopter, the LiDAR system Scout-16 that has a Velodyne VLP-16 multiple spinning sensors (technical specification in Table 1), the Inertial Measurement Unit (IMU) OEM-ADIS16488 and 3 Global Navigation Satellite System (GNSS) antennas NovAtel OEM6. The overlap between flight strips was 20%, and the mean velocity of the UAV was 5 m/s. By recording two returns, and after quality control of the point cloud (see [34]) in mean, 97.14 points/m^2 were captured in a total of 713,777,230 points that occupied 19 GB of disk space.

Table 1 – Technical specifications of the LiDAR system (Phoenix LiDAR Systems, 2018).

Sensor	Laser	Performance Specifications	Other
LiDAR sensor VLP-16	Class 1 Eye safe	Measurement rate ~300,000 pts/s	Net weight 590 g
No. of lasers/planes 16	Wavelength 903 nm	Max. operation range 100 m	Power consumption 8 W
Horizontal field of view 360°	Dual Returns (strongest and last)	Max range accuracy ±3 cm	
Vertical field of view -15° to +15°	Beam Divergence 3mrad	Range resolution 2 mm	
Horizontal Resolution 0.1° – 0.4°	Firing Repetition Rate 55.296 s/18.2 kHz	Footprint at 100m 30 cm	
Vertical resolution 2°	Maximum output energy 31 watts (0.19 micro joules)		
Rotation Rate 5 Hz – 20 Hz			

The software LiDARMill of Phoenix LiDAR Systems was used to combine the IMU and GNSS data to generate smoothed and accurate trajectories. Afterwards, it automatically detected and omitted turns and calibration patterns. The processing was completed by geo-referencing the data, minimising offsets from multiple flight lines (strip adjustment), and exporting the aligned data into the industry-standard LAS format. The geo-referencing of the data in the projection system PT-TM06 ETRS89 and the Altimetric Datum of Cascais, was done by using 25 GNSS base stations and the closest national network of permanent GNSS stations. The method used was the Post-Processed Kinematic (PPK). The LiDAR point cloud was then processed with the software TerraScan of Terrasolid. By filtering it, a Digital Terrain Model (DTM) was produced, and it's quality assessed by using 277 ground control points. The residuals in Z were obtained using the software TerraScan by which the Z values for points located at the same X and Y locations as the ground control points were interpolated using the triangle facets made with the three closest points in the filtered cloud. Table 2 lists the obtained Root Mean Square Error (RMSE) and other related quality data. It should be noticed that the filtering process has a high impact on the final accuracy. Filtering based on the Axelsson filter [48], implemented in

TerraScan, was used. A Digital Surface Model (DSM) was also produced in a raster format with both ground and non-ground points.

Table 2 – Final RMSE in altimetry and other related quality data.

Mean (m)	RMSE (m)	Minimum and maximum residuals (m)	Percentage of the residuals smaller than 0.40 m
-0.04	0.15	-0.49;0.60	99%

The laser sensor used, with a wavelength of 903 nm (Table 1) does not penetrate water and, therefore, is not appropriate to characterise the river channel [41, 49]. Thus, the topography of the river and the artificial channel was carried out through a bathymetric survey using a single beam sonar system. The integration of a Digital Terrain Model (DTM), produced with LiDAR, with a river bathymetric survey is recognised to provide better flood model outputs [50]. Cross-sections of the channel (Figure 2a) surveyed approximately every 75 m by the Portuguese National Hydrographic Institute were merged to the LiDAR DTM. To characterise the flood-prone area topography for hydrodynamic modelling, a DTM with 0.4 m spatial resolution was produced (Figure 2b).

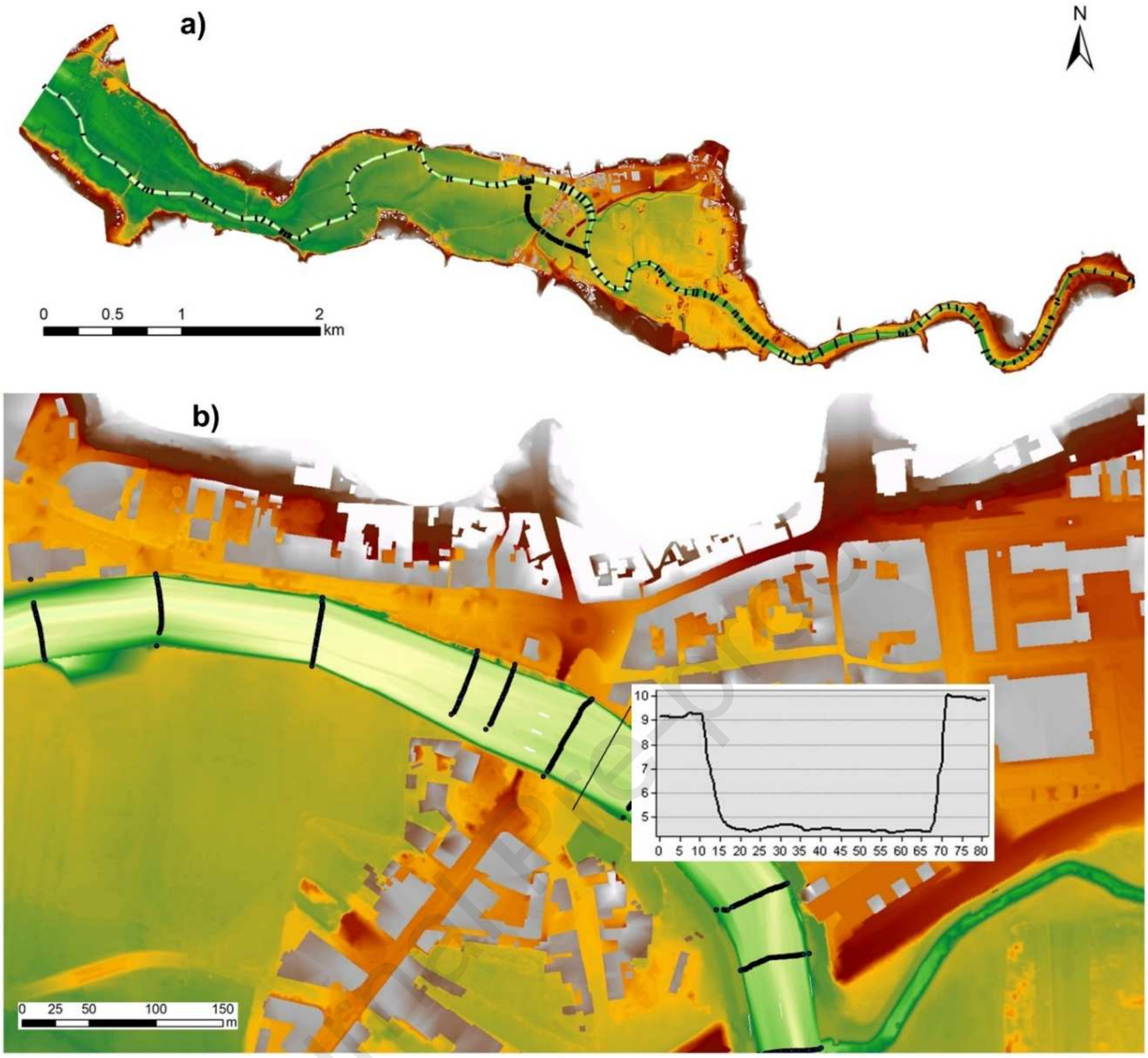

Figure 2 – a) Bathymetry cross-sections along the river channel; b) Detailed final cross-section used in the flood model.

The thematic information related to the study area is needed to derive the Manning's coefficients used to calibrate, validate and run the hydrodynamic model. To this end, an orthophoto was produced. Its integration with the LiDAR data allows one to produce a 3D land cover map. The orthophoto with an average ground sampling distance equal to the image pixel size of 3.5 cm was produced with the software Pixel4D. To this end, there were used 4,565 images acquired with the camera FC6310_8.8_4864x3648 (RGB) mounted on a Phantom 4 Pro, in October 2017, with two flights for redundancy at an average height of 110 m and 150 m.

According to the characteristics of the study area, seven land cover classes concerning seven object types were considered to be sufficient to characterise the terrain obstacle to the flow: three related to vegetation, namely, low vegetation, shrubs, and trees; three related to human-made objects, i.e., roads, walls, and buildings; and the other type being water (treated separately). The 3D land cover map production starts with a coarse classification using a normalised Digital

Surface Model (nDSM) produced by subtracting the LIDAR DTM from the LIDAR DSM so that Normalised Heights (NH) are obtained. These are used to group first the land cover obstacles into three height classes based on their height values above the bare terrain surface. The classification is then fine-tuned by further subdividing each of the three height classes into two for a total of six classes. This fine-tuning is done using a Green Leaf index image produced with the orthophoto.

The three height classes contain; one low features, the other near-ground features and the third high features. Thus, a height class image is produced by assigning the pixels in the LIDAR nDSM to a height class depending on their NH value. So, pixels with NH < 0.2 m are assigned to the low features class, like roads and low vegetation. Pixels with NH heights between 0.2 m and 2.0 m are assigned to the near-ground features, like walls and shrubs, whereas pixels with NH > 2.0 m are assigned to the high features class, like buildings and trees. A "Green Leaf Index" (GLI) image can then be produced using the reflection difference between the orthophoto's red, blue and green channels. The green channel is the dominant channel in vegetation. Therefore, the GLI is calculated to emphasise the green colour to distinguish healthy vegetation from other features. It is based on the following expression [51].

$$GLI = (2 * GREEN - RED - BLUE) / (2 * GREEN + RED + BLUE) \quad 1)$$

The resulting pixel values range from between -1.0 and 1.0, while positive values tend to represent healthy vegetation, and negative ones other features. Due to changing light and environmental conditions, the threshold to distinguish the classes is not always located around zero [52]. The integration of the height classes with the Green Leaf index image allows one to classify the features into six classes further namely: i) for the low features class: low vegetation and roads, ii) for the near-ground features class: walls and bushes, and iii) for the high features class: trees and buildings.

To obtain a reliable classification of the river and artificial channel without interfering with other areas´classification, their margins were manually digitised using the orthophoto. With ArcMap software, polygons were created according to the river channel boundaries, which were then transformed into raster data to be used as the input layer for classification. All the pixels inside the polygons were classified as water. Besides, to this 3D cover map were added the bridge's pillars of 5 bridges. These were manually digitised with the Microstation software using the LiDAR point cloud.

3 Design of the Flood Forecast and Alert System

FFAS proposes a framework for flood forecasting, taking advantage of state-of-the-art technology to acquire high-resolution and high accuracy terrain data, like LiDAR, NWP data, and Web-GIS services.

Water level observations from Alhandra hydrometric gauge are measured in real-time using the datalogger Gealog SG. This gauge is equipped with GPRS transmission data and programmed to automatically send the data to an FTP server set up for the purpose. The National Environmental monitoring network data is obtained through a programming routine and sent to the FTP server. The system runs the NWP automatically, computing hyetographs (with 15 minutes resolution) used as input to the calibrated Hydrologic Engineering Center - Hydrologic Modeling System (HEC-HMS) [53] and the Hydrologic Engineering Center - River Analysis System (HEC-RAS) [54, 55] models. Coupling these three models is a powerful tool to assess water levels and flood extent due to a high precipitation event. Runoff forecasting is accomplished using the HEC-HMS model that deals with the basic water balance equation considering the critical processes that govern runoff and can model a rainfall-runoff event. HEC-RAS 2D hydrodynamic model can simulate the channel's flow [54].

FFAS outputs are hourly depth, velocity and flood extent maps forecasts for the next 72 hours (3 days). FFAS takes about 90 minutes to provide hourly forecasts for water level and flood extents for the next 72 hours. Along with the updates of the NWP (section 3.1) from Clima@UA (http://climetua.ua.pt, Group of Meteorology and Climatology), simulation results are updated promptly (every six hours). Using a Web-GIS service, the water depth information is assigned to cells of 0.4 x 0.4 m^2 and aggregated into three classes of alert levels (section 3.4) displayed on the forecast flood extent map. Users can freely access the Web-GIS platform to view those alert maps and decide whether to prepare for possible flooding. Users registered at the platform can also choose buildings that, when within the forecast flood extent, will trigger the system to send an email to the user. Furthermore, whenever the water depth reaches specific values in predefined strategic hot spots , alerts are released to the Civil Protection Authorities that have determined them. The system's general layout is presented in Figure 3, and the system components will be described in the following sections.

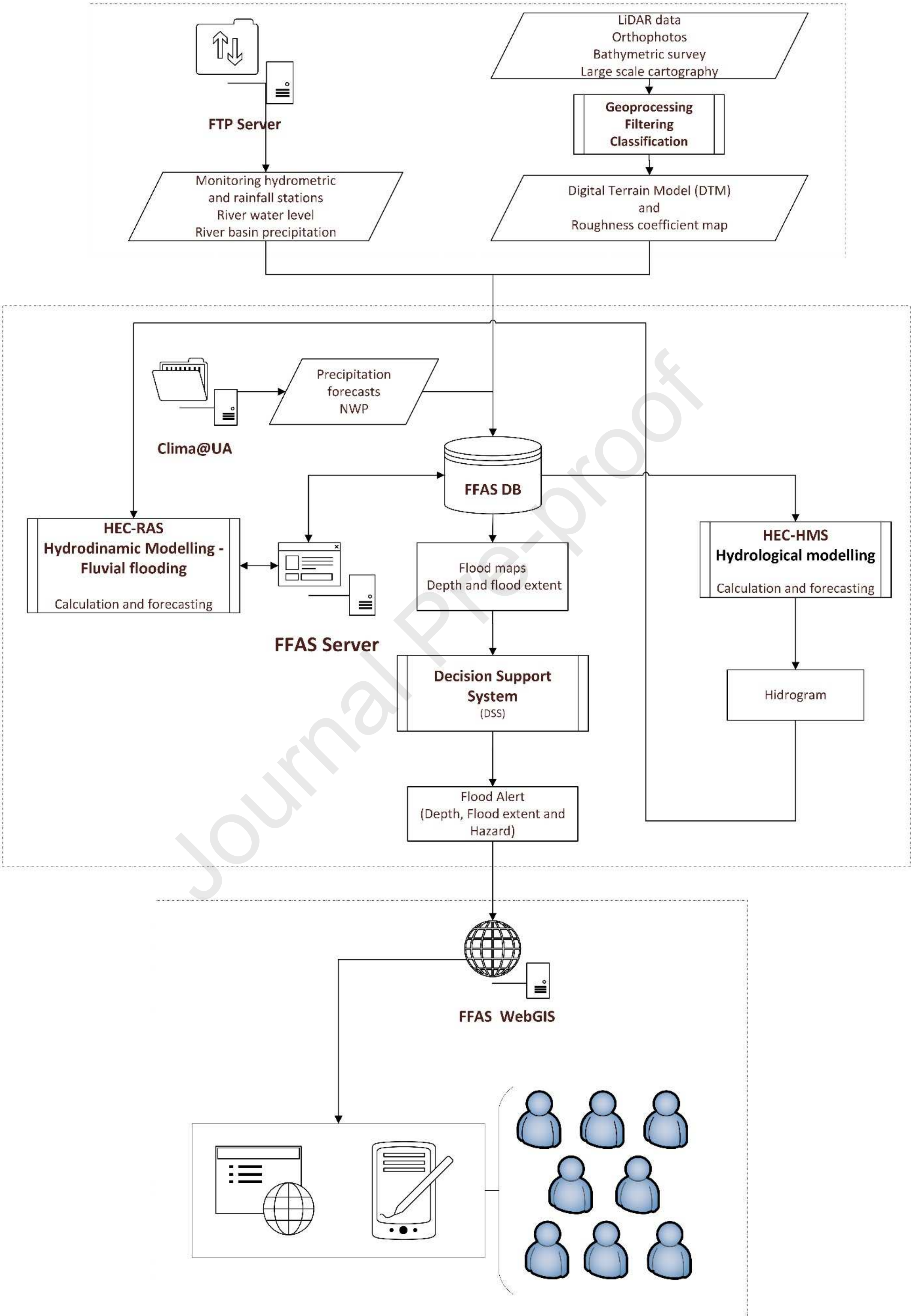

Figure 3. Flood forecast and alert system framework.

The FFAS was completed in July 2019 and is now undergoing operational tests. The continually recorded data are also likely to improve the hydrological and hydrodynamic models' calibration.

3.1 Numerical weather prediction

The ability of Numerical Weather Prediction (NWP) models to forecast rainfall has increased significantly in recent years [11, 56-59]. The NWP model used in FFAS is the Weather Research and Forecasting (WRF) Model with Advanced Research WRF (ARW) dynamic core version 2.2 [60]. WRF is a next-generation, limited-area, non-hydrostatic mesoscale modelling system, with vertical terrain-following eta-coordinate designed to serve operational and forecasting and atmospheric research needs. The WRF-ARW model has been widely used for simulating precipitation processes, both in the forecast [61] and in diagnostic modes [62]. It has also been successfully used in Portugal to test sensitivity to parameterisations of two different model operational configurations [63].

The WRF-ARW model was forced with the 6-hourly forecast meteorological fields of the Global Forecast System (GFS) from the United States of America's National Center for Environmental Prediction (NCEP). The GFS model has an approximated horizontal resolution of 0.5º × 0.5º, and the vertical domain extends from a surface pressure up to 0.27 hPa, discretised in 64 vertical unequally-spaced sigma levels, from which 15 levels are below 800 hPa, and 24 levels are above 100 hPa.

The WRF-ARW model was configured with two nested domains, with resolutions of 25 km and 5 km, respectively. The vertical discretisation consists of 27 terrain levels, following eta levels.

The following physical parameterisation schemes were used: WRF Single Moment 6 class scheme microphysics [64]; Dudhia shortwave radiation [65]; Rapid Radiative Transfer Model (RRTM) longwave radiation model [66]; MM5 similarity surface layer scheme [60], Yonsei University (YSU); planetary boundary layer scheme [67]; Noah Land Surface Model [68]; Grell-Freitas Ensemble scheme for cumulus parameterisation [69]; MM5 similarity surface layer scheme [70]; and Yonsei University Planetary Boundary layer [64]. These sets of parameterisations have been tested and used in the operational weather forecast system for Portugal available at the University of Aveiro (http://climetua.ua.pt, Group of Meteorology and Climatology), and several other studies of extreme events [71-73].

Nevertheless, post-processing must be performed based on observations to derive predictive fit and the numerical weather model performance [74]. Forecasts with WRF are performed every 6 hours for a temporal horizon of 72 hours. Precipitation is extracted at 15-minute intervals. The validation of these forecasts was performed based on the national meteorological network observations for the Varziela meteorological station events (Figure 1b). The validation methodology was as follows:

- Every day the system received four forecasts runs for the next eight days;
- For each forecast, 1 hour, 3 hours, 6 hours, 12 hours and 24 hours of precipitation accumulation was calculated, resulting in 5 forecast series for each forecast run;
- For each forecast series, a lagged series was constructed;
- Integrated and lagged precipitation series were also obtained for the observations;
- Model performance is evaluated by comparing simulated with measured hourly rainfall above a minimum 0.1mm/h threshold;
- The forecast results were computed for a grid over the river basin. As the observation data available are only for one rain gauge, three numerical experiments were made to compare the forecast with the observation series: i) the grid forecast results interpolated by IDW; ii) the grid forecast results interpolated by Thyssen Polygons, and iii) the nearest grid point;
- The results were assessed with the statistical test p-value (p=0.001; p=0.01 and p=0.05).

The results are promising, although more events must be assessed. According to the results achieved so far, the numerical experiment with the Thyssen polygons interpolation technique gave the best results in the forecast validation.

For example, the correlation for the different rainfall integrations corresponding to the period between 00:00UTC 7 March 2019 and 00:00UTC 29 April 2019 is presented in Figure 4.

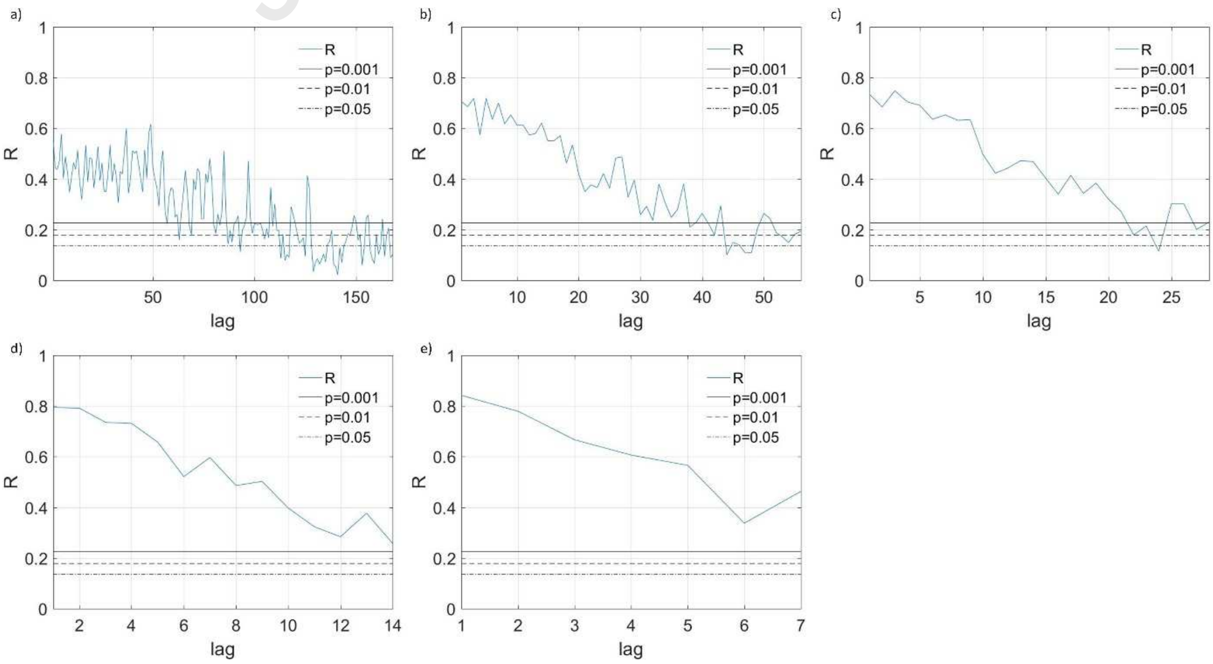

Figure 4. Statistical p-value (p=0.001; p=0.01 and p=0.05) of the correlations (R)between forecast and observed rainfall with 1- a), 3- b), 6- c), 12- d) and 24-hours e) accumulation for the period between 7th of March and 29th April 2019.

For 1 hour accumulation, the correlations between forecasts and observations were considered statistically significant until the lag 54, which corresponds to 2.25 days lead time. For the 3 hours accumulation, the lead time statistically significant is four days (lag 32). For the 6 hours accumulation, the lead-time statistically significant is 5.5 days (lag 22). For the 12 and 24 hours accumulation, the lead time statistically significant is eight days forecast. According to these results, the chosen lead time was three days.

3.2 Hydrological modelling

Rainfall-Runoff models help to visualise water systems' response to meteorological events and are crucial to increase flood-warning time in flood alert systems. The HEC-HMS model is an event-based hydrological model that computes dendritic watersheds' runoff response by describing physical and meteorological properties. It includes mathematical models for all the hydrological components that conceptually represent watershed behaviour such as infiltration loss, precipitation transformation into runoff hydrographs (direct runoff), channel routing, and baseflow. Hydrographs can be used either directly or in conjunction with other software for several studies, including flood forecasting.

HEC-HMS uses separate models to represent each component of the runoff process. The meteorological component is the computational unit by which precipitation input is distributed spatially and temporally over the basin.

The precipitation is subject to losses modelled by the precipitation loss component. In this study, the Soil Conservation Service (SCS) Curve Number (CN) loss method was used. The CN for each sub-basin was computed using land use and soil type data. The resulting excess precipitation contributes either to direct runoff or to baseflow. The transformation of excess precipitation into runoff was performed using the SCS unit hydrograph (UH) method, and the baseflow constant monthly method was selected. The routing component simulates the direct runoff and baseflow entering the river channels and the translation and flow attenuation. The lag (time difference between the maximum peak of precipitation and the maximum peak of flow) routing model was implemented.

The hydrologic elements shown in Figure 5 are derived from the DTM presented in section 2 for the basin. The CN uses the thematic map for the basin, also discussed in section 2. Four of the sub-basins have water level records.

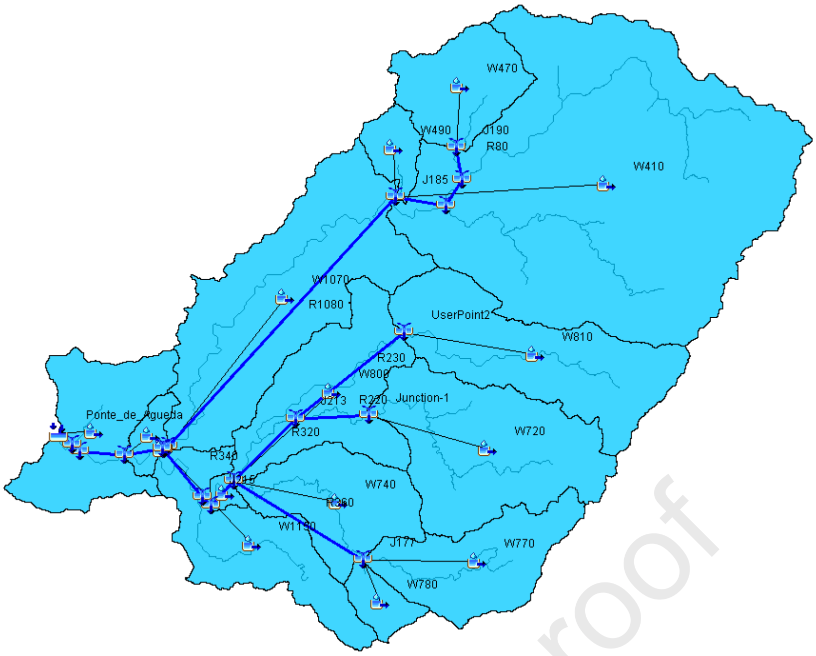

Figure 5. HEC-HMS Águeda River basin model including all the sub-basins, junctions and river elements.

Eleven years (2007–2018) of hourly rainfall data recorded at the three rainfall gauges mentioned in section 2 (Ponte de Águeda, Ponte Redonda and Ribeiro) were used to calibrate the hydrologic model (eight events). The calibration process was executed automatically by the HEC-HMS "Optimization Trial" tool, with the Univariate Gradient optimisation algorithm and minimising the Peak-Weighted RMSE objective function for each river section, as well as for all sub-basins. An independent set of data (five events) was used to validate the model.

A hydrologic parameter sensitivity analysis was conducted to assess the parameters that the calibration process must fine-tune to increase the model's predictive accuracy. The calibration is focused on the most sensitive parameters, including the Curve Number (CN), initial abstraction (Ia), SCS lag, lag routing and recession constant (RC).

Initial parameters values were set according to standard hydrology textbooks. Several statistical model performance evaluation criteria are employed for model parameters' optimisation (in the sense of calibration) and for comparing the models' accuracy [75-78]. The Nash-Sutcliffe Efficiency (NSE) index is a reliable statistic for assessing the hydrologic model's goodness-of-fit. NSE values ranging from 69% to 88% during calibration and 63% to 77% during validation indicate that the model runoff estimates could be considered in good agreement with the observed runoff.

3.3 Hydrodynamic modelling

River Analysis System (RAS) is a modelling tool developed by the U.S. Army Corps of Engineering’s Hydrologic Engineering Center (HEC) for analysing hydraulics of river systems. HEC-RAS can perform one (1D) and two-dimensional (2D) unsteady flow simulations. The model includes two computational solvers, the 2D Diffusion Wave and the 2D Saint Venant using an Implicit Finite Volume solution algorithm. The implicit solution method allows for larger computational time-steps than explicit solution methods. In addition, the finite volume method provides a greater degree of stability and robustness over traditional finite difference and finite element methodologies.

The computations were made with the full 2D unsteady flow model that can predict flow, velocity and water levels. Figure 6a) presents the 2D mesh of the domain, including the upstream and downstream boundary conditions (red lines) and the break lines (brown lines) associated with high ground or roads in the study area. From Figure 6b), it is possible to differentiate the 2D mesh cell size and a detail of the refinement zones (blue lines) that encompass the river and artificial channels and the river banks.

a)

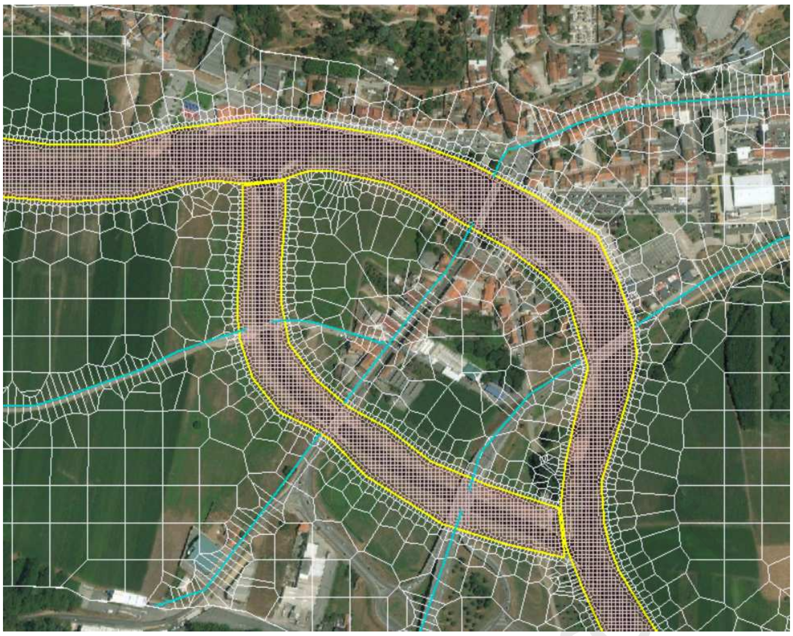

b)

Figure 6. a) HEC-RAS computational domain representing the 2D mesh, the break lines (light blue), refinement regions (yellow) and boundary conditions (red). b) Detail of the 2D mesh in the river and the floodplain.

The primary input of HEC-RAS 2D for performing hydraulic analysis are geometric and flow data. All the geometric data were imported into HEC-RAS 2D, and the quality of data was verified. Since the selected flow regime was subcritical, the boundary condition was defined only at the river's downstream end (Figure 6a) by the normal depth (considering the river bed's slope). In this study, the 2D Diffusion Wave solver was considered since it takes a shorter computational time than the Full Momentum equation. In developing the 2D model, the computational runtime must be considered because FFAS must update the flood forecasts every 6 hours. Taking this into consideration, and after several model verification tests, the final model features are:

- The 2D mesh with 38 544 cells;
- The 2D mesh with a cell size of 50 m in the flood area and 5 m in the river (Figure 8b);
- The hydrograph output interval of 1 hour;
- The computation time step interval of 10 seconds. This time step enables the Courant number of 1.0 (or less), which is required for accuracy and stability;
- The simulation with a duration of 72 h plus 48 h to warm-up.

The model upstream boundary requires a volumetric inflow rate (gauges during calibration and HEC-HMS hydrograph during forecast). The model also requires an imposed water surface elevation at the downstream boundary condition calculated at the downstream outflow using a normal depth condition, with a slop of down reach water surface set at 0.0024 m/m, the same as the bed slope.

Calibration of the riverbed and banks Manning's roughness is performed against the hourly-observed water levels at the gauge Ponte Águeda (section 2) for the same hydrological model calibration period (eight events). The calibrated model was then validated for five other events. The objective function used for calibration was also the NSE. The NSE efficiency values range from 56% to 75% during calibration and from 48% to 72% during validation. The channel roughness was fixed at 0.055 $m^{1/3}$/s, a value considered consistent with tables of Manning's n values in standard texts [79].

3.4 Design of client-server application

The client-server application displays the flood forecast extent and water levels and sends alert messages. Its server component consists of a GeoServer [80] that runs on a Tomcat application server [81] and a website developed using Laravel [82] that is hosted on an Apache server [83] running PHP. This component is responsible for receiving and storing the results of the hydrometric model's execution, namely the GeoServer using the Postgresql Database Management System (DBMS) [84].

In turn, the client application is executed in the user's browser. This component provides a graphical interface that is built using OpenLayers [85], Bootstrap [86] and AngularJS [87]. The information made available to the client is acquired through the invocation of Web Services published on the server. These services allow access to the forecasts and Web Services published by the Laravel website permitting registered users' management.

Users can access the web site with two different perspectives: assessing the forecast water level and visualise the flood extent, and/or they can make a registration with an email address and a selection of buildings to be alerted about if they are forecast to be flooded (Figure 7).

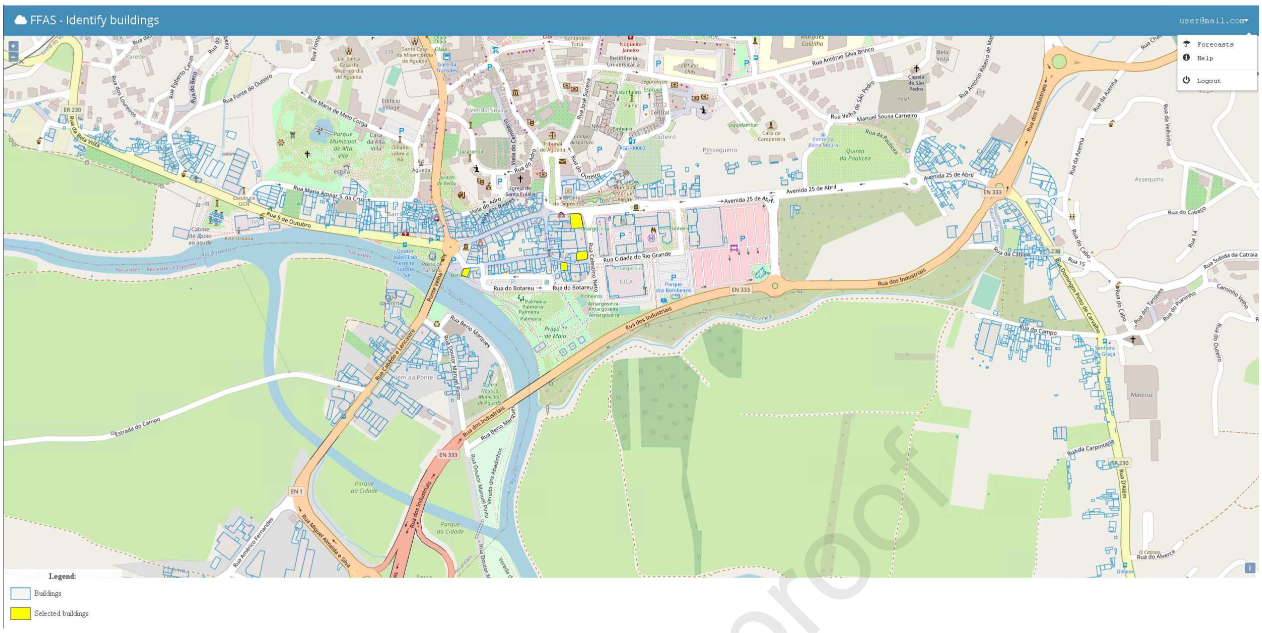

Figure 7. FFAS membership window where the end-users can select the buildings' locations to receive email flood alerts.

The Web-GIS module receives the water level outputs from the hydrodynamic model and classifies them into three predefined classes:

- Medium hazard: 0 m <water depth < 0.5 m;
- High hazard: 0.5 m ≤water depth < 1.0 m;
- Very High hazard: water depth ≥ 1.0 m.

Users can access the website http://ffas.web.ua.pt/previsao (Figure 8) and scroll the hourly water level and flood extent for three days forecast.

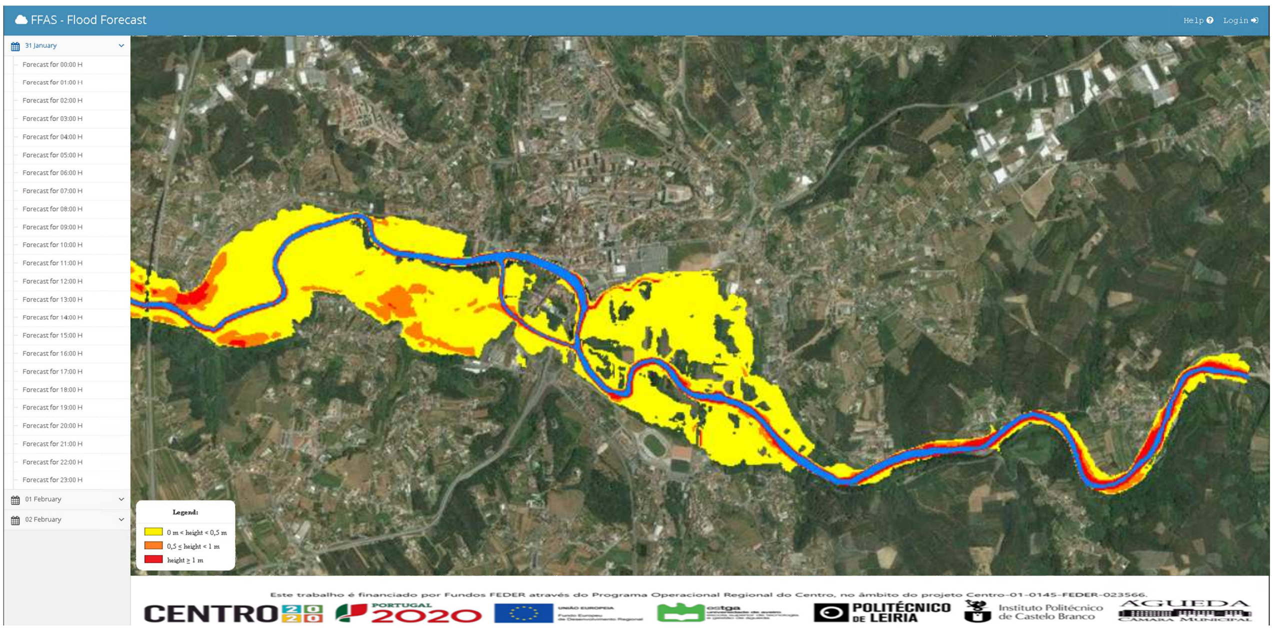

Figure 8. Hourly flood extent and water level FFAS Web-GIS layout.

The user can make a zoom to their area of concern and, due to the high-resolution DTM, it is possible to apprehend the flooded areas (Figure 9) quickly and, if necessary, undertake individual flood resilience measures. FFAS high resolution allows the end-users to be more identified with the flood hazard in their community.

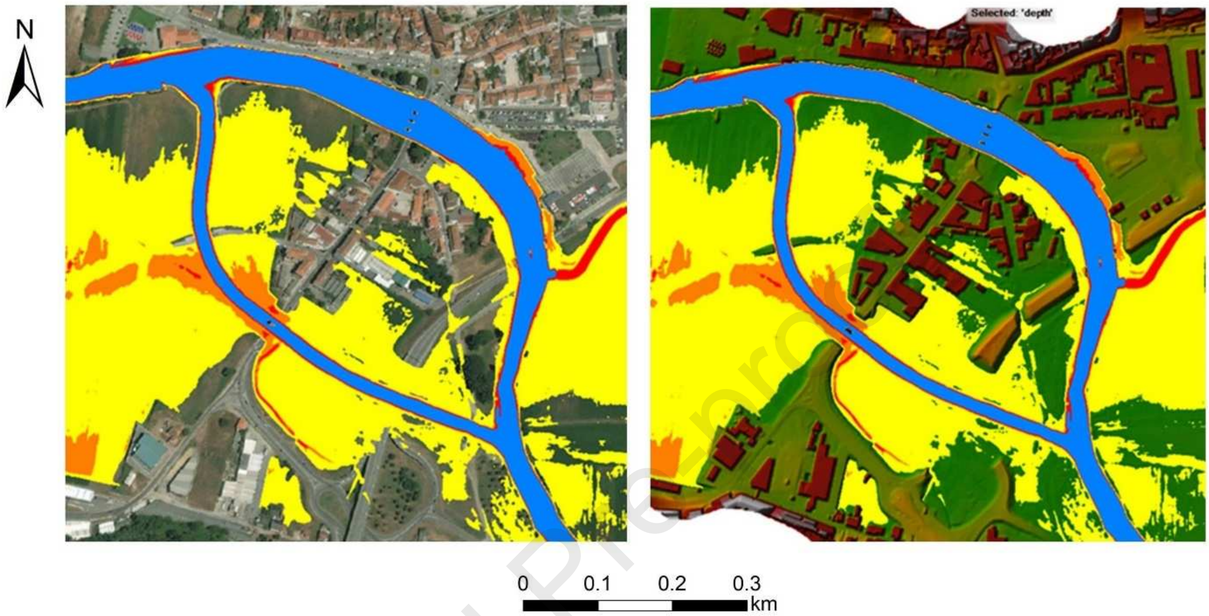

Figure 9. Detail of a flood extent and water level classes in Águeda downtown taken from the FFAS system (flood event between 31st January and 1st of February 2019).

4 Model performance analysis in operational forecasting

The first operational results are very encouraging. FFAS has already demonstrated its potential. The system forecasts performance was assessed with a rainfall event between 31 January and 1 of February of 2019. Figure 8 shows the flood extent forecast for that flood event six-hour in advance. The system successfully predicted the flooding that struck Águeda almost 72 hours in advance.

Post-flood maximum water levels were surveyed on the day of the event by a team of the Topographic Services of Águeda municipality hall. The comparison between the forecasts and the observations is based on flood extent measures. These measures are the fit statistics F^1 (equation 1), F^2 (equation 2) and the Bias (equation 3)

$$F^1(\%) = \frac{A}{A+B+C} \times 100 \quad (1)$$

$$F^2(\%) = \frac{A-B}{A+B+C} \times 100 \quad (2)$$

$$Bias(\%) = \frac{A+B}{A+C} \times 100 \quad (3)$$

where A represents the area being flooded according to both the system and observations (true positive), B is the overestimated area by the system (false positive), and C is the underestimated area by the system (false negative).

The fit statistics have been used in many previous studies [45, 88-93] and are useful to validate models against binary (wet/ dry) pattern data. The Bias gives a measure of over-or underestimation of the system in terms of the total wet area. A Bias value of 100% implies that the estimated wet area has the same size as the observed wet area; however, it does not provide information on these two areas (Figure 10). The F measures allow a quantitative comparison of the estimated flood extent to the maximum water levels surveyed. The F^1 has been modified in F^2 to penalise, additionally, overestimation of flood extent [94].

Figure 10 shows that the fit statistics and bias values calculated for 13 flood extent forecasts from 00:00UTC January 29 until 00:00UTC February 1, 2019 (for the period between 00:00UTC February 1 and 00:00UTC February 2, 2019) corroborate the good performance of the system considering the percentage of the flood area forecast for the given flood event. Although the first and tenth forecasts, respectively, 72 and 18 h previous to the peak flood event, present a similarity with the peak flood extent of only about 50% and 70%, respectively, the statistic measures improved substantially for the other forecasts, with some variations between 80% and 90%. These results allow concluding that the system accurately forecasts the flood event with an appropriated lead time, which allows the authorities and the population to take the necessary protection measures. The scientific community can easily understand that the results come with a certain level of uncertainty due to the inherent uncertainty of the input data, e.g. the DTM and the structure and parameterisation of the weather forecast, hydrological and hydrodynamic models. For ordinary citizens and even for the authorities that may not be so straightforward, the Web-GIS platform has a disclosure statement alerting to the displayed information's uncertainties.

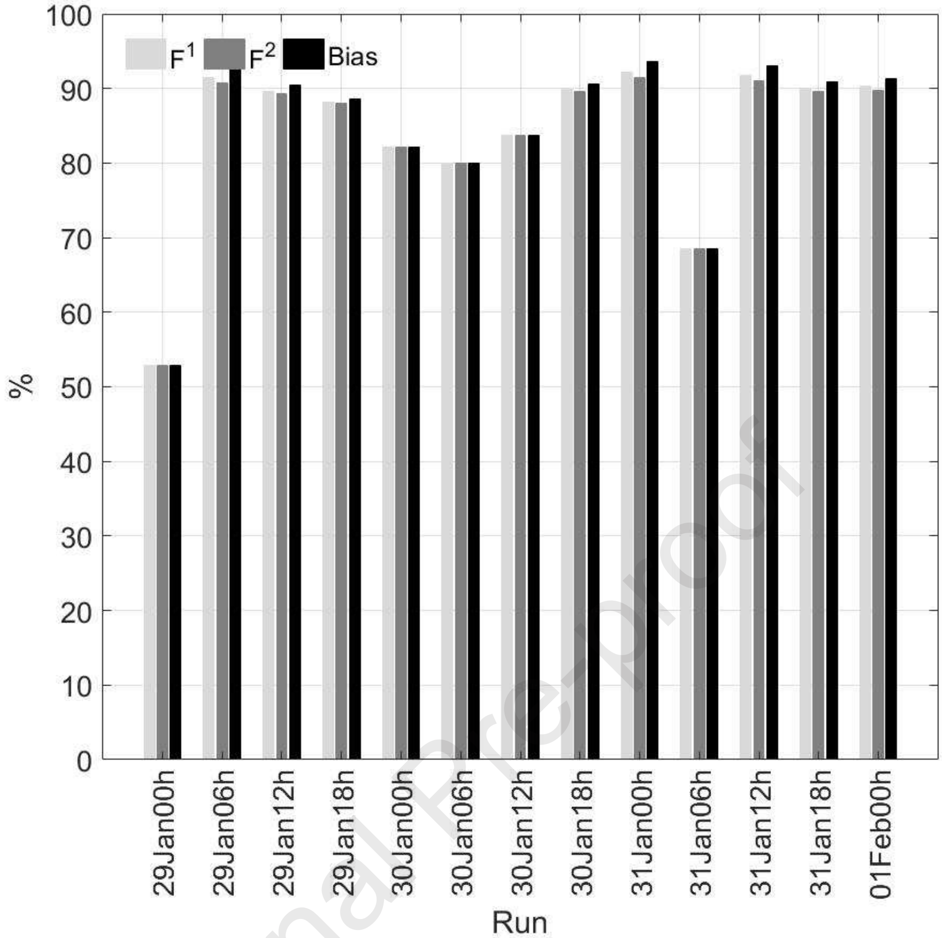

Figure 10. Chronological forecasts flood extent fit statistic measures (F^1; F^2 and Bias) for the event between January 31 and February 1, 2019.

In the flood forecast area, two water level gauges are available with hourly observations in the study area: Ponte de Águeda and Alhandra. To assess FFAS performance at river scale, a comparison between the water level observations and 13 forecasts for the period mentioned above is made and presented in Figure 11.

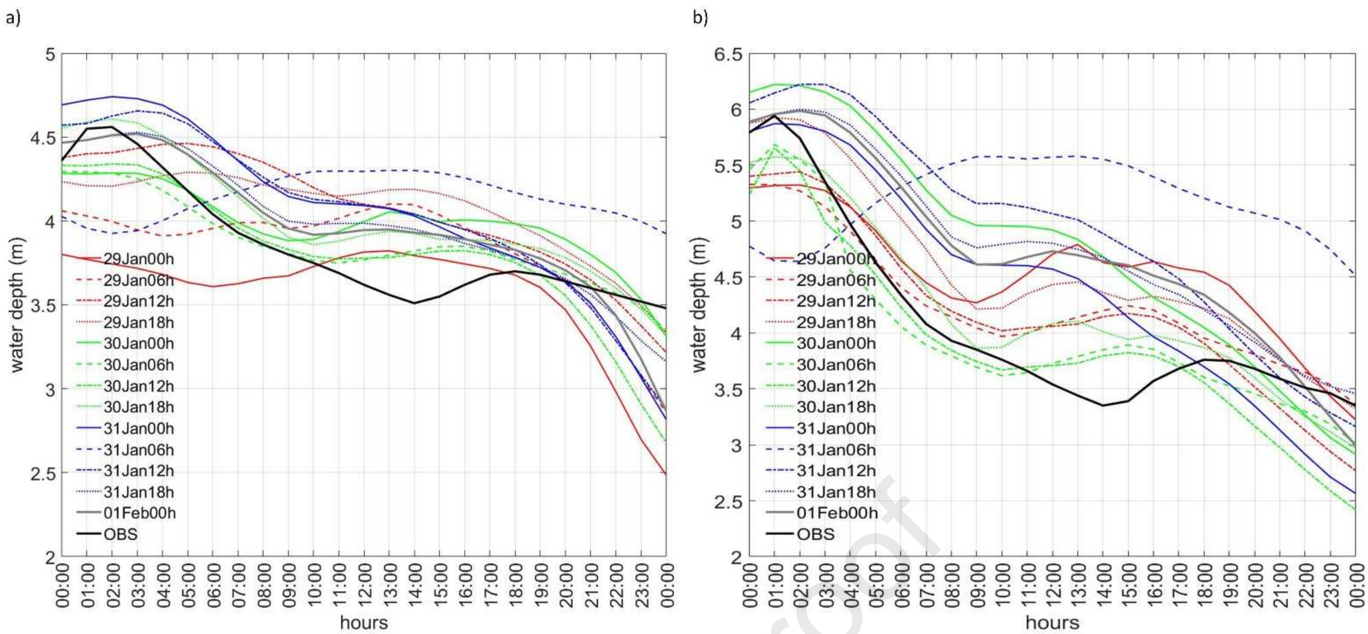

Figure 11. Water level observations (black line) and chronological forecasts (grey gradient lines) for the event between January 31 and February 2, 2019, at Ponte de Águeda (a) and Alhandra (b) water level gauges.

The last forecast run (00:00 UTC on February 1, 2019) accurately forecast the maximum water level in both water level gauges. Several other runs (with the exception for runs 1 and 10, respectively 72 h and 18 h before the peak flood event) simulated accurately (-8% to 12% at Ponte de Águeda and -8% to 10% at Alhandra) the water level at its maximum depth which is concordant with the results in Figure 10. During the flow recession, the system overestimates the water level, namely at Alhandra but not to levels that meant flooding over the riverbanks. At the Ponte de Águeda water level located at Águeda city centre (the most flood-prone area), the forecast post-peak water level inaccuracy is much lower. With the continuous data gathering done by the implemented system, both hydrological and hydrodynamic models will be improved, and these inaccuracies will certainly decrease.

5 Discussion

In this section, the FFAS is discussed by comparing it to other EWS available in an operational mode. It is important to emphasise that this study's framework is an operational system and not an experimental one. FFAS aims to be a technical solution to a frequent problem in Águeda city and elsewhere. When replicating the system, costs must be taken into account; the system is developed with freely available software so that the main costs will relate to the acquisition of terrain and bathymetric topography.

The system described in [29] can be considered similar to FFAS using NWP and freely available hydrologic and hydrodynamic (2D) models. Nevertheless, it is not known if bathymetry is used, and although the simulation time is similar to that of FFAS, it is for a much smaller numerical simulation domain. Furthermore, the weather forecast is only updated once a day, and it is not clear whether the results are disseminated. FFAS differs from Delft-FEWS because it relies on pre-established models, but both have a modular approach and allow for high-resolution flood forecast.

Another key element of an EWS to produce an accurate flood forecast is the terrain topography that should portray all the relevant terrain features that interfere with the water flow. One way to achieve this requirement is to use a DTM with high-resolution in the inundation area and river bed. The DTM used by FFAS was produced with data acquired with LiDAR in a UAV, which is still a relatively new technology. The LiDAR data acquired with a UAV was four times less expensive than that acquired with an aircraft while resulting in comparable accuracy. The obtained accuracy of 15 cm in altimetry is conforming to the standards for the production of DTM at large scales. It is superior to that obtained with UAV photogrammetry with a consumer-grade camera for LiDAR penetrates through vegetation [95].

Another aspect that should be highlighted is the 3D land cover map. It describes the surface in the form of topographic objects. These objects are clearly defined and associated with one type of land use embedded in the hydrodynamic model with a defined roughness. Usually, a roughness map is produced manually by associating manning roughness coefficients to a land cover map. In the FFAS a very detailed 3D land cover map produced automatically is used, although, due to the lack of events with water levels available at the inundation area, the roughness was not yet calibrated.

The HEC-HMS is a fully-featured multiple purpose surface hydrologic model that can be used to perform flood forecasting, successfully implemented worldwide in several research works [24, 28, 29, 96-98]. The HEC-RAS has been successfully applied, showing to be suitable for studying and analysing flood propagation and flood mapping [26, 27, 45, 99-102]. The models HEC-HMS and HEC- RAS were chosen due to several factors that have a significant impact on the flood forecast: a) forecasting time step versus the time of concentration; b) the robustness of the models, which allows avoiding sudden instabilities, and consequently lack of forecasts; c) the low computational time since FFAS updates forecasts every 6 hours. Despite the uncertainty associated with modelling, the hourly NSE during calibration and validation could be considered suitable, as shown by other EWS [26, 27]. The system, although in operational mode, needs to be continuously assessed when recent flood events occur. Since the system was implemented, only two flood events took place (February and December of 2019), but water levels from Ponte de Águeda gauge were not available during the second event. The system will need to be periodically assessed; in case of large forest fires (or other significant land-use change), the hydrological model parameterisation must be changed accordingly. The same continuous effort must be undertaken with the hydrodynamic model to ensure that flood events, flood extent, and water levels will be accurately forecast for the following flood events. As more flood events occur and are assessed, it is expected that system confidence outcomes increases and more citizens will use it.

While NWP data can be downloaded in a few seconds, and the hydrologic model can run in a few minutes, the system's real bottleneck is the hydrodynamic model. The FFAS hydrodynamic model was set up to optimise simulation time without compromising the numerical stability. The mesh dimension, the equation set, the time step, the warm-up period, and all the parameterisation were optimised to a maximum Courant number of one to ensure the numerical stability and run with a lead-time suitable for operational decision-making. The WRF model is one of the world references and most used; nevertheless, it needs to be adjusted to perform best for the region. The results obtained so far indicated that the NWP could forecast the intense precipitation. As FFAS is operational and more flood events occur, precipitation forecasts can be improved, considering the integration with radar to increase flood warnings' accuracy. Several forecast systems use probabilistic forecasting models considered more skilful than deterministic forecasting [103-107]. Computational constraints still affect the resolution of the probabilistic forecasts. For the time being, including probabilistic forecasting is not a FFAS priority. Due to the high-resolution of the hydrodynamic model and the current computational capabilities, the deterministic approach has advantages due to the high hydrodynamic detail and the time to provide the 72h forecasts updated every 6 hours. Some of the systems that presently use a probabilistic approach use low-resolution and only hydrological modelling [13], 1D-hydraulic models [108] and flood threshold [109, 110].

The European Flood Awareness System (EFAS) [13] uses an ensemble of weather forecasts and a hydrological model to provide twice-daily forecasts of river flow and flood warnings as early as ten days before a flood event [111-113]. The weather forecasts are used to drive the hydrological model set up on a 5 km grid cell of the EFAS domain. The EFAS forecast and products are only available to EFAS partners. Only the EFAS forecasts and products more than 30 days old are freely available to all. For the 31st January 2019 event forecast, and as may be seen in Figure 9, whereas FFAS shows a significant detail in the flood extension (and water level), the resolution of EFAS is coarser due to the 5 km grid cell. FFAS forecast the flood with a three days lead-time, although when consulting the EFAS historical forecast records, only on the

31st was issued a flood warning with a 10% probability in the next 48h (in the two previous days, no flood forecast was issued for the next 48h). Besides, there are no forecast water levels. Notwithstanding EFAS being very important at the national level, the flood-prone areas' forecasts must be complemented at a local level with systems like FFAS.

6 Conclusions

The technological developments implemented in FFAS for Águeda city include numerical weather forecasting coupled with hydrodynamic modelling, the usage of very high-resolution spatial data, and full integration of the system into a Web-GIS platform highlight the advances in operational fluvial flood forecasting. This modelling framework is essential in the context of the legislative drivers' alterations made for flood forecasting and alert. The system is currently operational, and the preliminary results are considered acceptable.

FFAS manages to couple WRF with the hydrologic HEC-HMS rainfall-runoff and the HEC-RAS 2D hydrodynamic models. This coupling process plays a pivotal role to accurately forecast water levels and flood extents for three days with updates every six hours. All models were calibrated to obtain the parameters' values representing flood event responses over the study area. Furthermore, the models were validated with other events.

FFAS uses Web-GIS services to create a platform were the forecast water levels aggregated into three alert levels are overlaid on the forecast flood extent and visualised in an image. Águeda civil protection services and citizens can freely access the Web-GIS platform to view those alert maps. If they choose to register at the platform, users can also choose buildings that will trigger the system to send an email if within the forecast flood extent. Furthermore, whenever the water depth reaches specific values in predefined strategic hot spots, alerts are released to the civil protection authorities. At the moment, the emergency services are the primary end-user, although several citizens are already registered. As the system is operational, we intend to take participatory meetings with the community to increase the application's penetration rate and inform them how to understand and make the best use of the forecasts. With the increased lead-time, the civil protection authorities, environmental authorities, and citizens can gain time to reduce damage and protect property and lives.

A reliable FFAS has to account for forecast uncertainty. Errors in forecast quality may be due to uncertainty in hydrological data, potential data errors, and improper optimisation of the models' parameters and model structure (spatial and temporal resolution). An important aspect of further research is the calibration of the NWP model. Comparing forecast and observed precipitation is decisive to the accuracy of the results. Some investment is needed to implement a rainfall gauge in the drainage basin and a water level gauge in the river near the city centre, so the system does not rely only on the Portuguese system SVARH data. Future work will also continuously assess the results as flood events occur and proceed to the models' parameterisation update whenever necessary. New features are intended to be implemented so FFAS will self-assess its performance by comparing observations(water level, rainfall and flood extent) to forecasts in specific locations chosen according to their flood risk based on the site vulnerability and damage costs.

Accurate flood modelling at high spatial-temporal resolution remains a significant challenge in hydrologic and hydraulic studies. It will undoubtedly require high-resolution terrain data. FFAS uses as input a DTM produced with a high-density LiDAR point cloud (around 100 points/m^2). LiDAR offers high density and very accurate terrain data by penetrating the vegetation. Accurate flood maps help design and implement flood risk management strategies and longer-term development plans. Preparedness activities and timely response can be undertaken if the forecast information also comes with the forecast flood level. The proposed flood forecast and alert system implemented on a Web-GIS is flexible to couple with pluvial hydrodynamic models as long the computational time is made compatible with the warning necessary lead-time.

We expect FFAS to be a useful decision support tool for Águeda civil protection that can be replicated elsewhere. Furthermore, the information obtained from FFAS, together with vulnerability assessment and damage curves, allow the estimation of flood damage that can be used by the insurances companies in the evaluation of the flood risk. By being a valuable tool to manage flood risk, we hope that it will also increase the citizens' resilience living in flood-prone areas. In the context of climate change, this aspect is even more relevant.

Funding: This work is supported by the Operational Programme of the Centre Region, in its FEDER component, in the ambit of the project Centro-01-0145-FEDER-023566 and by FCT/MCTES financial support to CESAM(UIDP/50017/2020+UIDB/50017/2020), through national funds.

References

1. Fernandez, P., S. Mourato, and M. Moreira, *Social vulnerability assessment of flood risk using GIS-based multicriteria decision analysis. A case study of Vila Nova de Gaia (Portugal).* Geomatics, Natural Hazards and Risk, 2015. **7**: p. 1367-1389.
2. Balica, S. and N.G. Wright, *Reducing the complexity of the flood vulnerability index.* Environmental Hazards, 2010. **9**(4): p. 321-339.
3. Paprotny, D., A. Sebastian, O. Morales-Nápoles, and S.N. Jonkman, *Trends in flood losses in Europe over the past 150 years.* Nature Communications, 2018. **9**(1): p. 1985.

4. Guha-Sapir, D., H. Ph., and B. R., *Annual Disaster Statistical Review 2014: The Numbers and Trends*. 2015, CRED: Brussels.
5. Alfieri, L., B. Bisselink, F. Dottori, G. Naumann, A. de Roo, P. Salamon, K. Wyser, and L. Feyen, *Global projections of river flood risk in a warmer world.* Earth's Future, 2017. **5**(2): p. 171-182.
6. Alfieri, L., P. Burek, L. Feyen, and G. Forzieri, *Global warming increases the frequency of river floods in Europe.* Hydrol. Earth Syst. Sci., 2015. **19**(5): p. 2247-2260.
7. Forzieri, G., L. Feyen, S. Russo, M. Vousdoukas, L. Alfieri, S. Outten, M. Migliavacca, A. Bianchi, R. Rojas, and A. Cid, *Multi-hazard assessment in Europe under climate change.* Climatic Change, 2016. **137**(1): p. 105-119.
8. Winsemius, H.C., Jeroen C.J.H. Aerts, Ludovicus P.H. van Beek, Marc F.P. Bierkens, A. Bouwman, B. Jongman, Jaap C.J. Kwadijk, W. Ligtvoet, Paul L. Lucas, Detlef P. van Vuuren, and Philip J. Ward, *Global drivers of future river flood risk.* Nature Climate Change, 2016. **6**(4): p. 381-385.
9. Dennis John, P., *Flood Warning Systems and Their Performance*. 2019, Oxford University Press.
10. Merkuryeva, G., Y. Merkuryev, B.V. Sokolov, S. Potryasaev, V.A. Zelentsov, and A. Lektauers, *Advanced river flood monitoring, modelling and forecasting.* Journal of Computational Science, 2015. **10**: p. 77-85.
11. Givati, A., E. Fredj, and M. Silver, *Chapter 6 - Operational Flood Forecasting in Israel*, in *Flood Forecasting*, T.E. Adams and T.C. Pagano, Editors. 2016, Academic Press: Boston. p. 153-167.
12. Jain, S.K., P. Mani, S.K. Jain, P. Prakash, V.P. Singh, D. Tullos, S. Kumar, S.P. Agarwal, and A.P. Dimri, *A Brief review of flood forecasting techniques and their applications.* International Journal of River Basin Management, 2018. **16**(3): p. 329-344.
13. Thielen, J., J. Bartholmes, M.H. Ramos, and A. de Roo, *The European Flood Alert System – Part 1: Concept and development.* Hydrol. Earth Syst. Sci., 2009. **13**(2): p. 125-140.
14. Demargne, J., L. Wu, S.K. Regonda, J.D. Brown, H. Lee, M. He, D.-J. Seo, R. Hartman, H.D. Herr, M. Fresch, J. Schaake, and Y. Zhu, *The Science of NOAA's Operational Hydrologic Ensemble Forecast Service.* Bulletin of the American Meteorological Society, 2013. **95**(1): p. 79-98.
15. Kundzewicz, Z.W., *Floods: lessons about early warning systems*, in *Late lessons from early warnings: science, precaution, innovation.*, E. Report, Editor. 2013, European Environment Agency (EEA): Copenhagen. p. 347-368.
16. Kull, D., R. Mechler, and S. Hochrainer-Stigler, *Probabilistic cost-benefit analysis of disaster risk management in a development context.* Disasters, 2013. **37**(3): p. 374-400.
17. Mechler, R., *Reviewing estimates of the economic efficiency of disaster risk management: opportunities and limitations of using risk-based cost–benefit analysis.* Natural Hazards, 2016. **81**(3): p. 2121-2147.
18. Demeritt, D., S. Nobert, H.L. Cloke, and F. Pappenberger, *The European Flood Alert System and the communication, perception, and use of ensemble predictions for operational flood risk management.* Hydrological Processes, 2012. **27**(1): p. 147-157.
19. Cranston, M.D. and A.C.W. Tavendale, *Advances in operational flood forecasting in Scotland.* Proceedings of the Institution of Civil Engineers - Water Management, 2012. **165**(2): p. 79-87.
20. United Nations, *Sendai Framework for Disaster Risk Reduction 2015-2030*. 2015, United Nations Office for Disaster Risk Reduction: Geneva, Switzerland.
21. Romang, H., M. Zappa, N. Hilker, M. Gerber, F. Dufour, V. Frede, D. Bérod, M. Oplatka, C. Hegg, and J. Rhyner, *IFKIS-Hydro: an early warning and information system for floods and debris flows.* Natural Hazards, 2011. **56**(2): p. 509-527.
22. Saramago, M., *Redes de Monitorização Hidrometeorológicas.* Recursos Hídricos, 2017. **38**(1): p. 33-39.
23. Rao, K.H.V.D., V.V. Rao, V.K. Dadhwal, G. Behera, and J.R. Sharma, *A distributed model for real-time flood forecasting in the Godavari Basin using space inputs.* International Journal of Disaster Risk Science, 2011. **2**(3): p. 31-40.
24. Azam, M., H.S. Kim, and S.J. Maeng, *Development of flood alert application in Mushim stream watershed Korea.* International Journal of Disaster Risk Reduction, 2017. **21**: p. 11-26.
25. Bartholmes and Todini, *Coupling meteorological and hydrological models for flood forecasting.* Hydrol. Earth Syst. Sci., 2005. **9**(4): p. 333-346.
26. Mai, D. and F. Smedt, *A Combined Hydrological and Hydraulic Model for Flood Prediction in Vietnam Applied to the Huong River Basin as a Test Case Study.* Water, 2017. **9**: p. 879.
27. Lamichhane, N. and S. Sharma, *Development of Flood Warning System and Flood Inundation Mapping Using Field Survey and LiDAR Data for the Grand River near the City of Painesville, Ohio.* Hydrology, 2017. **4**(2).
28. Lagmay, A.M.F.A., B.A. Racoma, K.A. Aracan, J. Alconis-Ayco, and I.L. Saddi, *Disseminating near-real-time hazards information and flood maps in the Philippines through Web-GIS.* Journal of Environmental Sciences, 2017. **59**: p. 13-23.
29. González-Cao, J., O. García-Feal, D. Fernández-Nóvoa, J.M. Domínguez-Alonso, and M. Gómez-Gesteira, *Towards an automatic early warning system of flood hazards based on precipitation forecast: the case of the Miño River (NW Spain).* Nat. Hazards Earth Syst. Sci., 2019. **19**(11): p. 2583-2595.

30. Silvestro, F., L. Rossi, L. Campo, A. Parodi, E. Fiori, R. Rudari, and L. Ferraris, *Impact-based flash-flood forecasting system: Sensitivity to high resolution numerical weather prediction systems and soil moisture.* Journal of Hydrology, 2019. **572**: p. 388-402.
31. Werner, M., J. Schellekens, P. Gijsbers, M. van Dijk, O. van den Akker, and K. Heynert, *The Delft-FEWS flow forecasting system.* Environmental Modelling & Software, 2013. **40**: p. 65-77.
32. Brandão, C., M.M. Saramago, T. Ferreira, S. Cunha, S. Costa, T. Alvarez, F.F.d. Carvalho, M. Silva, C. Duarte, F. Braunschweig, D. Brito, L. Fernandes, E. Jauch, and R.P. Silva, *Elaboração de Cartografia Específica sobre Risco de Inundação para Portugal Continental. Relatório Final, Volume 1 - Memória Descritiva*. 2014, Agência Portuguesa do Ambiente: Lisbon, Portugal. p. 260.
33. Zêzere, J.L., S. Pereira, A.O. Tavares, C. Bateira, R.M. Trigo, I. Quaresma, P.P. Santos, M. Santos, and J. Verde, *DISASTER: a GIS database on hydro-geomorphologic disasters in Portugal.* Natural Hazards, 2014. **72**(2): p. 503-532.
34. Pereira, L.G., P. Fernandez, S. Mourato, J. Matos, C. Mayer, and F. Marques, *Quality Control of Outsourced LiDAR Data Acquired with a UAV: A Case Study.* Remote Sensing, 2021. **13**(3).
35. Nunes, J.P., S.H. Doerr, G. Sheridan, J. Neris, C. Santín, M.B. Emelko, U. Silins, P.R. Robichaud, W.J. Elliot, and J. Keizer, *Assessing water contamination risk from vegetation fires: Challenges, opportunities and a framework for progress.* Hydrological Processes, 2018. **32**(5): p. 687-694.
36. Arnone, E., D. Pumo, A. Francipane, G. La Loggia, and L.V. Noto, *The role of urban growth, climate change, and their interplay in altering runoff extremes.* Hydrological Processes, 2018. **32**(12): p. 1755-1770.
37. Brunner, M.I., A.E. Sikorska, and J. Seibert, *Bivariate analysis of floods in climate impact assessments.* Science of The Total Environment, 2018. **616-617**: p. 1392-1403.
38. NASA, USGS, and NGA, *Shuttle Radar Topography Mission (SRTM) Version 3.0 Global 1 arc second* 2014, U.S. Geological Survey (USGS): Sioux Falls, South Dakota.
39. Direção-Geral do Território, *Especificações técnicas da Carta de Uso e Ocupação do Solo (COS) de Portugal Continental para 2018. Relatório Técnico*. 2019, Direção-Geral do Território: Lisboa, Portugal.
40. Panagos, P., *The European Soil Database.* GEO: connexion, 2006. **5**: p. 32-33.
41. Cook, A. and V. Merwade, *Effect of topographic data, geometric configuration and modeling approach on flood inundation mapping.* Journal of Hydrology, 2009. **377**(1-2): p. 131-142.
42. Yalcin, E., *Assessing the impact of topography and land cover data resolutions on two-dimensional HEC-RAS hydrodynamic model simulations for urban flood hazard analysis.* Natural Hazards, 2020. **101**(3): p. 995-1017.
43. Vozinaki, A.-E.K., G.G. Morianou, D.D. Alexakis, and I.K. Tsanis, *Comparing 1D and combined 1D/2D hydraulic simulations using high-resolution topographic data: a case study of the Koiliaris basin, Greece.* Hydrological Sciences Journal, 2017. **62**(4): p. 642-656.
44. Lim, N.J. and S.A. Brandt, *Flood map boundary sensitivity due to combined effects of DEM resolution and roughness in relation to model performance.* Geomatics, Natural Hazards and Risk, 2019. **10**(1): p. 1613-1647.
45. Horritt, M.S. and P.D. Bates, *Evaluation of 1D and 2D numerical models for predicting river flood inundation.* Journal of Hydrology 2002. **268**: p. 87-99.
46. Di Baldassarre, G. and A. Montanari, *Uncertainty in river discharge observations: a quantitative analysis.* Hydrol. Earth Syst. Sci., 2009. **13**(6): p. 913-921.
47. Fewtrell, T.J., P.D. Bates, M. Horritt, and N.M. Hunter, *Evaluating the effect of scale in flood inundation modelling in urban environments.* Hydrological Processes, 2008. **22**(26): p. 5107-5118
48. Axelsson, P., *Processing of laser scanner data-algorithms and applications.* ISPRS Journal of Photogrammetry and Remote Sensing, 1999. **54**: p. 138-147.
49. Hohenthal, J., P. Alho, J. Hyyppä, and H. Hyyppä, *Laser scanning applications in fluvial studies.* Progress in Physical Geography: Earth and Environment, 2011. **35**(6): p. 782-809.
50. Schumann, G., P. Matgen, M.E.J. Cutler, A. Black, L. Hoffmann, and L. Pfister, *Comparison of remotely sensed water stages from LiDAR, topographic contours and SRTM.* ISPRS Journal of Photogrammetry and Remote Sensing, 2008. **63**(3): p. 283-296.
51. Hunt, E.R., P.C. Doraiswamy, J.E. McMurtrey, C.S.T. Daughtry, E.M. Perry, and B. Akhmedov, *A visible band index for remote sensing leaf chlorophyll content at the canopy scale.* International Journal of Applied Earth Observation and Geoinformation, 2013. **21**: p. 103-112.
52. Louhaichi, M., M.M. Borman, and D.E. Johnson, *Spatially Located Platform and Aerial Photography for Documentation of Grazing Impacts on Wheat.* Geocarto International, 2001. **16**(1): p. 65-70.
53. Scharffenberg, B., M. Bartles, T. Brauer, M. Fleming, and G. Karlovits, *Hydrologic Modeling System HEC-HMS User's Manual*. 2018, U.S . Army Corps of Engineers Institute for Water Resources Hydrologic Engineering Center (CEIWR-HEC): Davis, CA.
54. Brunner, G.W. and CEIWR-HEC, *HEC-RAS River Analysis System, 2D Modeling User's Manual-Version 5.0*. 2016, U.S . Army Corps of Engineers Institute for Water Resources Hydrologic Engineering Center (CEIWR-HEC): Davis, CA. p. 171.

55. Brunner, G.W. and CEIWR-HEC, *HEC-RAS River Analysis System User's Manual Version 5.0*. 2016, U.S . Army Corps of Engineers Institute for Water Resources Hydrologic Engineering Center (CEIWR-HEC): Davis, CA. p. 962.
56. Emerton, R.E., E.M. Stephens, F. Pappenberger, T.C. Pagano, A.H. Weerts, A.W. Wood, P. Salamon, J.D. Brown, N. Hjerdt, C. Donnelly, C.A. Baugh, and H.L. Cloke, *Continental and global scale flood forecasting systems.* WIREs Water, 2016. **3**(3): p. 391-418.
57. Mittermaier, M., N. Roberts, and S.A. Thompson, *A long-term assessment of precipitation forecast skill using the Fractions Skill Score.* Meteorological Applications, 2013. **20**(2): p. 176-186.
58. Givati, A., B. Lynn, Y. Liu, and A. Rimmer, *Using the WRF Model in an Operational Streamflow Forecast System for the Jordan River.* Journal of Applied Meteorology and Climatology, 2012. **51**(2): p. 285-299.
59. Liechti, K., L. Panziera, U. Germann, and M. Zappa, *Flash-flood early warning using weather radar data: from nowcasting to forecasting.* Hydrology and Earth System Sciences Discussions, 2013. **10**: p. 1289-1331.
60. Skamarock, W.C.K., J.B.; Dudhia, J.; Gill, D.O.; Barker, D.M.; Duda, M.G.; Huang, X.-Y.; Wang, W.; Powers, J.G., *A Description of the Advanced Research WRF Version 3*. 2008, National Center for Atmospheric Research: Boulder, CO, USA.
61. Weisman, M.L., C. Davis, W. Wang, K.W. Manning, and J.B. Klemp, *Experiences with 0–36-h Explicit Convective Forecasts with the WRF-ARW Model.* Weather and Forecasting, 2008. **23**(3): p. 407-437.
62. Cardoso Pereira, S., M. Marta-Almeida, A.C. Carvalho, and A. Rocha, *Extreme precipitation events under climate change in the Iberian Peninsula.* International Journal of Climatology, 2020. **40**(2): p. 1255-1278.
63. Ferreira, J., A.c. Carvalho, L. Carvalheiro, A. Rocha, and J. Castanheira. *Sensitivity of a simulated extreme precipitation event to spatial resolution, parametrisations and assimilation*. in *10th EMS Annual Meeting, 8th European Conference on applied Climatology*. 2010. Zurich, Switzerland.
64. Hong, S.-Y., Y. Noh, and J. Dudhia, *A New Vertical Diffusion Package with an Explicit Treatment of Entrainment Processes.* Monthly Weather Review, 2006. **134**(9): p. 2318-2341.
65. Dudhia, J., *Numerical Study of Convection Observed during the Winter Monsoon Experiment Using a Mesoscale Two-Dimensional Model.* Journal of the Atmospheric Sciences, 1988. **46**(20): p. 3077-3107.
66. Mlawer, E.J. and S.A. Clough. *On the extension of rapid radiative transfer model to the shortwave region*. in *Proceedings of the 6th Atmospheric Radiation Measurement (ARM) Science Team Meeting*. 1997. US Department of Energy, CONF-9603149.
67. Noh, Y., W.G. Cheon, S.Y. Hong, and S. Raasch, *Improvement of the K-profile Model for the Planetary Boundary Layer based on Large Eddy Simulation Data.* Boundary-Layer Meteorology, 2003. **107**(2): p. 401-427.
68. Kusaka, H., M. Tewari, J.W. Bao, and H. Hirakuchi. *Utilizing the coupled WRF/LSM/URBAN modeling system with detailed urban classification to simulate the urban heat island phenomena over the greater Houston area*. in *Fifth conference on urban environment*. 2004.
69. Grell, G.A. and S.R. Freitas, *A scale and aerosol aware stochastic convective parameterization for weather and air quality modeling.* Atmos. Chem. Phys., 2014. **14**(10): p. 5233-5250.
70. Zhang, D.-L. and R. Anthes, *A High-Resolution Model of the Planetary Boundary Layer—Sensitivity Tests and Comparisons with SESAME-79 Data.* Journal of Applied Meteorology, 1982.
71. Pereira, S.C., A.C. Carvalho, J. Ferreira, J.P. Nunes, J.J. Keizer, and A. Rocha, *Simulation of a persistent medium-term precipitation event over the western Iberian Peninsula.* Hydrol. Earth Syst. Sci., 2013. **17**(10): p. 3741-3758.
72. de Melo-Gonçalves, P., A. Rocha, and J.A. Santos, *Robust inferences on climate change patterns of precipitation extremes in the Iberian Peninsula.* Physics and Chemistry of the Earth, 2016. **94**: p. 114-126.
73. Viceto, C., S. Cardoso, M. Marta-Almeida, I. Gorodetskaya, and A. Rocha. *Assessment of future extreme climate events over the Porto wine Region*. 2017.
74. Bogner, K. and F. Pappenberger, *Multiscale error analysis, correction, and predictive uncertainty estimation in a flood forecasting system.* Water Resources Research, 2011. **47**(7).
75. Gupta, H.V., S. Sorooshian, and P.O. Yapo, *Toward improved calibration of hydrologic models: Multiple and noncommensurable measures of information.* Water Resources Research, 1998. **34**(4): p. 751-763.
76. Krause, P., D.P. Boyle, and F. Bäse, *Comparison of different efficiency criteria for hydrological model assessment.* Advances in Geosciences, 2005. **5**: p. 89-97.
77. Moriasi, D.N., J.G. Arnold, M.W. Van Liew, R.L. Bingner, R.D. Harmel, and T.L. Veith, *Model Evaluation Guidelines for Systematic Quantification of Accuracy in Watershed Simulations.* Transactions of the ASABE, 2007. **50**(3): p. 885-900.
78. Bhuiyan, H.A.K.M.M., H.; Powers, J.; Merzouki, A., *Application of HEC-HMS in a Cold Region Watershed and Use of RADARSAT-2 Soil Moisture in Initializing the Model.* Hydrology, 2017(4): p. 9.
79. Chow, V.T., *Open-Channel Hydraulics*. 1988: McGraw-Hill Inc.
80. Open Source Geospatial Foundation. *GeoServer*. 2020; GeoServer 2.17.1 [Available from: http://geoserver.org/.

81. The Apache Software Foundation. *Apache Tomcat*. 2020; Apache Tomcat® 9.x [Available from: http://tomcat.apache.org/.
82. Taylor Otwell. *Laravel*. 2020; Available from: https://laravel.com/.
83. The Apache Software Foundation. *Apache server* 2020; Apache®2.4.43 [Available from: https://www.apache.org/.
84. PostgreSQL Global Development Group. *PostgreSQL*. 2020; PostgreSQL 12:[Available from: www.postgresql.org.
85. FOSSA. *OpenLayers*. 2020; OpenLayers v6.3.1:[Available from: https://openlayers.org/.
86. MIT. *Bootstrap*. 2020; Bootstrap v4.5.0:[Available from: https://getbootstrap.com/.
87. MIT. *AngularJS*. 2020; angular 1.8.0:[Available from: https://angularjs.org/.
88. Horritt, M.S., *Development of physically based meshes for two-dimensional models of meandering channel flow*. International Journal for Numerical Methods in Engineering, 2000. **47**(12): p. 2019-2037.
89. Horritt, M.S. and P.D. Bates, *Predicting floodplain inundation: raster-based modelling versus the finite-element approach.* Hydrological Processes, 2001. **15**(5): p. 825-842.
90. Horritt, M.S. and P.D. Bates, *Effects of spatial resolution on a raster based model of flood flow* Journal of Hydrology, 2001. **253**(1-4): p. 239-249
91. Horritt, M.S., G. Di Baldassarre, P.D. Bates, and A. Brath, *Comparing the performance of a 2-D finite element and a 2-D finite volume model of floodplain inundation using airborne SAR imagery.* Hydrological Processes, 2007. **21**(20): p. 2745-2759.
92. Prestininzi, P., G. Di Baldassarre, G. Schumann, and P.D. Bates, *Selecting the appropriate hydraulic model structure using low-resolution satellite imagery.* Advances in Water Resources, 2011. **34**(1): p. 38-46.
93. Aronica, G., P.D. Bates, and M.S. Horritt, *Assessing the uncertainty in distributed model predictions using observed binary pattern information within GLUE.* Hydrological Processes, 2002. **16**(10): p. 2001-2016.
94. Hunter, N.M., P.D. Bates, M.S. Horritt, A.P.J. De Roo, and M.G.F. Werner, *Utility of different data types for calibrating flood inundation models within a GLUE framework.* Hydrology and Earth System Science, 2005. **9 (4)**: p. 412-430.
95. Salach, A., K. Bakuła, M. Pilarska, W. Ostrowski, K. Górski, and Z. Kurczyński, *Accuracy Assessment of Point Clouds from LiDAR and Dense Image Matching Acquired Using the UAV Platform for DTM Creation.* ISPRS International Journal of Geo-Information, 2018. **7**(9).
96. Joo, J., T. Kjeldsen, H.-J. Kim, and H. Lee, *A comparison of two event-based flood models (ReFH-rainfall runoff model and HEC-HMS) at two Korean catchments, Bukil and Jeungpyeong.* KSCE Journal of Civil Engineering, 2014. **18**(1): p. 330-343.
97. Halwatura, D. and M.M.M. Najim, *Application of the HEC-HMS model for runoff simulation in a tropical catchment.* Environmental Modelling & Software, 2013. **46**: p. 155-162.
98. Gül, G.O., N. Harmancıoğlu, and A. Gül, *A combined hydrologic and hydraulic modeling approach for testing efficiency of structural flood control measures.* Natural Hazards, 2010. **54**(2): p. 245-260.
99. Song, Y., Y. Park, J. Lee, M. Park, and Y. Song, *Flood Forecasting and Warning System Structures: Procedure and Application to a Small Urban Stream in South Korea.* Water, 2019. **11**(8): p. 1571.
100. Golian, S., J. Yazdi, M.L.V. Martina, and S. Sheshangosht, *A deterministic framework for selecting a flood forecasting and warning system at watershed scale.* Journal of Flood Risk Management, 2015. **8**(4): p. 356-367.
101. Patel, D.P., J.A. Ramirez, P.K. Srivastava, M. Bray, and D. Han, *Assessment of flood inundation mapping of Surat city by coupled 1D/2D hydrodynamic modeling: a case application of the new HEC-RAS 5.* Natural Hazards, 2017. **89**(1): p. 93-130.
102. Dimitriadis, P., A. Tegos, A. Oikonomou, V. Pagana, A. Koukouvinos, N. Mamassis, D. Koutsoyiannis, and A. Efstratiadis, *Comparative evaluation of 1D and quasi-2D hydraulic models based on benchmark and real-world applications for uncertainty assessment in flood mapping.* Journal of Hydrology, 2016. **534**: p. 478-492.
103. Cloke, H.L. and F. Pappenberger, *Ensemble flood forecasting: A review.* Journal of Hydrology, 2009. **375**(3): p. 613-626.
104. Pagano, T.C., A.W. Wood, M.-H. Ramos, H.L. Cloke, F. Pappenberger, M.P. Clark, M. Cranston, D. Kavetski, T. Mathevet, S. Sorooshian, and J.S. Verkade, *Challenges of Operational River Forecasting.* Journal of Hydrometeorology, 2014. **15**(4): p. 1692-1707.
105. Verbunt, M., A. Walser, J. Gurtz, A. Montani, and C. Schär, *Probabilistic Flood Forecasting with a Limited-Area Ensemble Prediction System: Selected Case Studies.* Journal of Hydrometeorology, 2007. **8**(4): p. 897-909.
106. Atger, F., *Verification of intense precipitation forecasts from single models and ensemble prediction systems.* Nonlin. Processes Geophys., 2001. **8**(6): p. 401-417.
107. Verkade, J.S. and M.G.F. Werner, *Estimating the benefits of single value and probability forecasting for flood warning.* Hydrol. Earth Syst. Sci., 2011. **15**(12): p. 3751-3765.

108. Addor, N., S. Jaun, F. Fundel, and M. Zappa, *An operational hydrological ensemble prediction system for the city of Zurich (Switzerland): skill, case studies and scenarios.* Hydrol. Earth Syst. Sci., 2011. **15**(7): p. 2327-2347.

109. Goodarzi, L., M.E. Banihabib, and A. Roozbahani, *A decision-making model for flood warning system based on ensemble forecasts.* Journal of Hydrology, 2019. **573**: p. 207-219.

110. Abebe, A.J. and R.K. Price, *Decision support system for urban flood management.* Journal of Hydroinformatics, 2005. **7**(1): p. 3-15.

111. Bartholmes, J.C., J. Thielen, M.H. Ramos, and S. Gentilini, *The european flood alert system EFAS – Part 2: Statistical skill assessment of probabilistic and deterministic operational forecasts.* Hydrol. Earth Syst. Sci., 2009. **13**(2): p. 141-153.

112. Pappenberger, F., M.H. Ramos, H.L. Cloke, F. Wetterhall, L. Alfieri, K. Bogner, A. Mueller, and P. Salamon, *How do I know if my forecasts are better? Using benchmarks in hydrological ensemble prediction.* Journal of Hydrology, 2015. **522**: p. 697-713.

113. Ramos, M.-H., J. Bartholmes, and J. Thielen-del Pozo, *Development of decision support products based on ensemble forecasts in the European flood alert system.* Atmospheric Science Letters, 2007. **8**(4): p. 113-119.

Declaration of interests

☒ The authors declare that they have no known competing financial interests or personal relationships that could have appeared to influence the work reported in this paper.

☐The authors declare the following financial interests/personal relationships which may be considered as potential competing interests: